Layering, bundling, and azimuthal orientations in dense phases of nucleosome core particles

2006 J. Phys.: Condens. Matter 18 11429

(http://iopscience.iop.org/0953-8984/18/50/003)

INSTITUTE OF PHYSICS PUBLISHING JOURNAL OF PHYSICS: CONDENSED MATTER

J. Phys.: Condens. Matter **18** (2006) 11429–11442 doi:10.1088/0953-8984/18/50/003

Layering, bundling, and azimuthal orientations in dense phases of nucleosome core particles

A G Cherstvy[1] **and R Everaers**[1,2]

[1] Max-Planck-Institut für Physik Komplexer Systeme, Nöthnitzer Straße 38, D-01187 Dresden, Germany
[2] Ecole Normale Supérieure de Lyon, 46 Allée d'Italie, 69364 Lyon Cedex 07, France

Received 8 August 2006, in final form 24 October 2006
Published 27 November 2006
Online at stacks.iop.org/JPhysCM/18/11429

Abstract

We propose an idea how the helical pattern of charges on the surface of DNA can affect electrostatic interactions of nucleosome core particles in their columnar and crystalline phases as well as in chromatin. For bilayers of nucleosomes, we suggest that mutual azimuthal orientations of neighbouring NCPs are quantized with the angle of $\approx\pi/4$. We suggest that a similar mechanism of DNA-mediated inter-nucleosome interactions might stabilize new chromatin-like bundled columnar phases of nucleosomes which have not yet been observed.

(Some figures in this article are in colour only in the electronic version)

1. Introduction

The elementary packaging unit of eukaryotic chromatin—the nucleosome—contains about $1\frac{3}{4}$ left-handed DNA superhelical turns wrapped around the net positively charged histone octamer. This structure is highly conserved in all organisms. The nucleosome core particle (NCP) is a wedge-like 'cylinder' with a diameter of ≈105 Å and a height of ≈60 Å. The crystal structure of NCP has been resolved using high-resolution by x-ray diffraction [1, 2]. The interaction of NCPs influences both the properties of dense phases of NCPs and the structure and properties of 30 nm chromatin fibre. The latter is still a matter of intensive debate [3–8].

These interactions can be investigated in particular in concentrated solutions of NCPs, with no linker DNA and no H1-histones present. Under appropriate conditions (the amount of simple salt, the presence of specific di- and tri-valent cations, external pressure of PEG, etc) a variety of NCP dense phases (columnar-lamellar, quasi-hexagonal, nematic) [9–12], NCP quasi-hexagonal crystals [13–16], as well as NCP arcs and cylinders [17] have been observed. In solutions of some di- and tri-valent salts, NCPs precipitate into very dense phases [11]; in solutions of NaCl, depending on the external osmotic pressure, a variety of phases are found [12]. All these dense phases imply some *inter-nucleosomal interactions*, but their nature and intensity are not fully understood.

1.1. NCP bilayer phase

In particular, cylindrical columns of NCPs are formed in concentrated NCP solutions ($\sim$250 mg ml^{-1}) via 'top-to-bottom' stacking of NCP–NCP interactions. Parallel columns of NCPs are then assembled into bilayers with two raws of columns, presumably due to attractive lateral interactions between the core particles [18]. The bilayer phase is observed at low salt concentrations, between $\sim$3 and $\sim$30 mM of NaCl and at external PEG osmotic pressure between 3 and 25 atm; the NCP concentration in this phase is $\sim$300 mg ml^{-1}. At these low salt conditions but at pressures $>$25 atm an inverse hexagonal NCP phase is observed where the bilayers are matched together, forming a honey-comb structure of NCP columns [10]. At higher salt amounts (35 mM of NaCl) the columnar lamellar phase coexists with the hexagonal phase, whereas at even higher salt concentration (50–150 mM of NaCl) and at 5–13 atm of PEG pressure the two-dimensional (2D) and three-dimensional (3D) ordered hexagonal and quasi-hexagonal (orthorhombic) NCP phases are observed [9], with concentration of NCPs up to $\sim$500 mg ml^{-1} and distances between NCPs in neighbouring columns of 110–115 Å. Note that the same structures are revealed without external osmotic stress [10]; the latter effectively produces an attractive component of NCP–NCP interaction and also has an effect of liquid crystalline ordering[3]. At low salt conditions (below 30 mM) and at an external pressure below $\sim$1 atm, isotropic solutions of NCP columns and of isolated NCPs are observed [10]. A strong dependence of the salt concentration indicates the importance of electrostatic interactions.

The bilayers of NCPs are separated by a layer of solvent, and the periodicity of such a columnar-lamella NCP phase is $D \approx$ 25–40 nm. The axis of NCP (the axis of DNA superhelix) is either parallel to the axis of the column or slightly tilted with respect to it [12][4]. The NCP dyad axes are oriented *on average* perpendicular to the bilayer plane pointing out into the solution, but they fluctuate within $\pm 35^\circ$ near this direction [18]; figure 1(b). The sides of NCPs with two DNA turns face inside the bilayer forming contacts with neighbouring NCPs via lateral 'side-to-side' interactions. These interactions—the main focus of this paper—are likely to orient the core particles in bilayers azimuthally, since NCPs have disordered orientations along an isolated NCP column [9, 18]. To our knowledge, no quantitative analysis of NCP azimuthal orientations in bilayers have been performed yet, although some investigations are underway [19].

1.2. Interactions

It has been suggested that positively charged histone tails, typically with a high fraction of arginine and lysine residues [20], protruding through the aligned minor grooves of DNA duplex wrapped in the NCP (supergroove), can cause an attraction between NCPs and also trigger azimuthal alignment of NCPs in bilayers [21]. A phenomenological model of such NCPs' orientational ordering in bilayers has been suggested [22], however without considering DNA-specific interactions. Computer simulations of this tail-bridging effect have also been performed [23]; see also [24]. The histone tails are known to interact electrostatically with wrapped nucleosomal DNA at low salt concentrations, whereas they are extended into the

[3] The position of the phase boundaries becomes shifted as the initial NCP concentration or external PEG pressure or as the salt concentration change. These shifts *studied together* can provide additional information on the intensity of NCP–NCP interactions.

[4] Note that x-ray diffraction analysis of NCP bilayers [9] does not allow us to determine unambiguously whether the NCP axes in bilayers are oriented along the bilayer plane or *tilted* with respect to the column axis. One can speculate that electrostatic interactions of wrapped DNAs can favour such a tilt. Indeed, if we consider now wrapped DNA as left-handed superhelices, the direction of tilt predicted in experiments indeed brings two DNA fragments on contacting chiral NCPs into a closer-to-parallel juxtaposition that would ensure a larger DNA–DNA interaction energy.

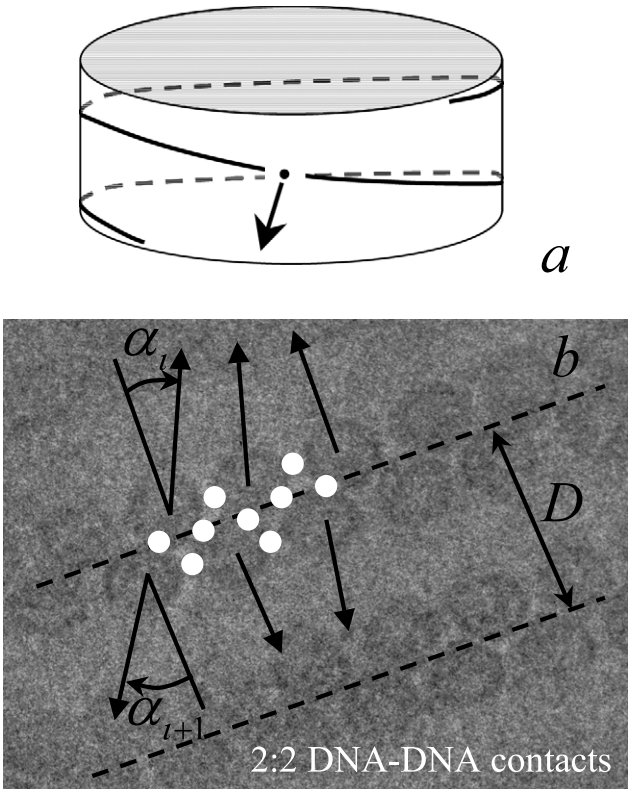

Figure 1. A sketch of NCP with the direction of the dyad axis (a) and a cryo-electron micrograph of the NCP bilayer (view along the bilayer plane; part of the image from 1c of [18] {reproduced with permission of the Biophysical Society and of A Leforestier}). Orientations of NCP dyad axes are shown by arrows. The 2:2 DNA–DNA contacts on neighbouring NCPs across and along the bilayer are shown by white circles.

solution at about 0.1–0.2 M of salt [25] and thus can bridge neighbouring NCPs. It is quite possible that histone tails are responsible for NCP bilayer formation and NCP azimuthal frustrations.

Here, we suggest that a nonhomogeneous helical distribution of charges on DNA can trigger this as well, imposing some constraints on inter-nucleosomal interactions. Separations between *DNA surfaces* on the neighbouring NCPs along the bilayer are ∼5 Å, whereas the distance for NCPs across two layers of NCPs in the same bilayer is ∼10–15 Å [18], figure 1(b) (whereas the separations between the bilayers D are much larger). These distances are of the order of the Bjerrum length, $l_B \approx 7$ Å, and of the Debye screening length at physiological salt conditions. As we show in the next section, strong electrostatic DNA–DNA interactions are detected at these distances, suggesting considerable DNA-mediated interactions of NCPs within the bilayers as well.

2. Electrostatics of DNA and NCP

2.1. DNA

The theory of electrostatic interaction of *parallel* charged helical molecules such as DNA has been developed recently in a series of papers [26–36]. This theory takes explicitly into

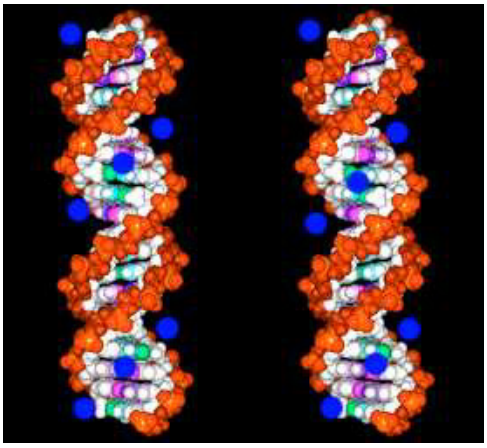

Figure 2. Electrostatic zipper motif of DNA–DNA attraction: the closest charges on juxtaposed DNAs have opposite signs. B-DNA phosphate strands are in red; the cations adsorbed in DNA major groove are shown schematically in blue.

account the *helical* symmetry of DNA charges and DNA low-dielectric core, on the level of the linear Poisson–Boltzmann equation [26]. The results of the theory and its modifications have been applied successfully to the description of several puzzling DNA-related phenomena, including the intensity of intermolecular forces [26, 29], the decay length of short- and long-range DNA–DNA repulsion [29], temperature-dependent [29] and sequence-specific [30] DNA condensation, electrostatic recognition of DNA sequences [28], interaction-induced DNA torsional deformations [30, 36], DNA melting in assemblies [31], DNA conformational transitions [32, 33] (see also [34]), and DNA toroidal condensation [35].

The theory predicts in particular that DNAs can attract each other via *zipper-like registration* along their contact between the phosphate charges (−) on one DNA and cations (+) adsorbed in the grooves of another DNA [26, 27]; see figure 2. This attraction occurs in theory at high degrees of DNA charge neutralization by the adsorbed cations, i.e. when intermolecular *net*-charge repulsion between DNAs is relatively weak. Attraction typically exists in the range of DNA–DNA interaxial separations of $R = 25$–35 Å (i.e. at ∼5–15 Å between the DNA surfaces), both in the theory [26, 29] (see the green curve in figure 6) and in the osmotic stress experiments [37]. The attraction decays with separation between the molecules *more quickly* than the common Debye–Hückel repulsion of uniformly charged rods [38]. The strength of attraction depends on the DNA charge distribution—where and how much cations are adsorbed on DNA—and it is more pronounced when a large fraction of DNA charge is neutralized by the cations (θ is close to unity) and when cations reside in the DNA major groove (f is close to 0). Cation adsorption both in DNA grooves and on the phosphate strands can be treated in the theory; in the text we consider for simplicity only the adsorption into grooves. This intermolecular attraction is reminiscent of DNA–DNA attraction due to correlations in profiles of condensed counterions proposed long ago by Oosawa [39] and developed in a number of recent papers [40]. Our DNA–DNA electrostatic interaction theory however *explicitly* considers DNA charge periodicity, which determines the periodicity of charge density waves along the DNA. Although below we concentrate on the effects of electrostatics on DNA–DNA and NCP–NCP interactions, other forces can act between closely positioned DNA (for instance, the hydration forces [37] of removing organized water molecules upon approaching DNA surfaces).

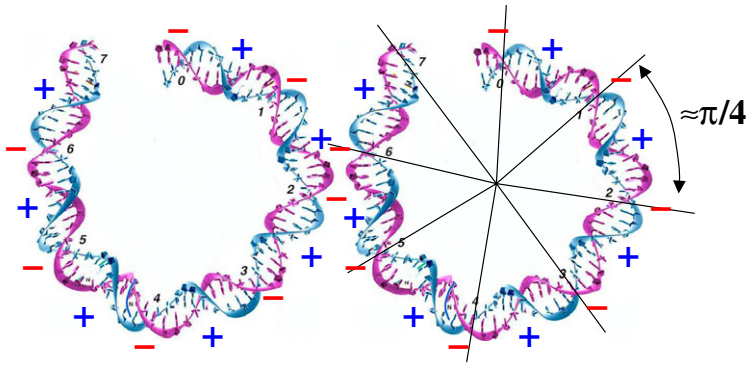

Figure 3. Two interacting NCPs and zipper of charges along the wrapped DNA, viewed along the axis of NCP superhelix. The positions where DNA minor grooves point outside the NCP are shown. DNA phosphates are marked as red charges; cations adsorbed in a DNA major groove are in blue. There are about eight full DNA turns per DNA super-turn in NCPs.

To a leading approximation, the interaction energy of parallel DNA fragments depends in a $-\cos(\delta\varphi)$ fashion on DNA mutual azimuthal rotation at an angle $\delta\varphi$ [26]. Thus, upon an axial shift of one DNA with respect to another, their interaction energy has a maximum at $\delta\varphi = \pi$ and a minimum at $\delta\varphi = 2\pi$ (the latter is equivalent to a shift by DNA helical pitch $H = 34$ Å). These orientational-dependent interactions were shown to cause peculiar DNA azimuthal frustration in dense ($R \lesssim 30$ Å) columnar hexagonal DNA assemblies [30]. Experimentally, similar orientational disordering upon squeezing of columnar DNA assemblies has also been detected [41]. Azimuthal disordering of NCPs in bilayers and quasi-hexagonal phases upon an increase in the external pressure is observed as well, as follows from the broadening of corresponding diffraction peaks [9][5].

2.2. NCP

Some tendencies of DNA-mediated NCP–NCP interactions are similar to those for parallel DNA in solution. One indication for this are similarities in the condensation and resolubilization behaviour of DNA [42] and of NCPs [9, 12] upon the addition of DNA-condensing cations (spermine, spermidine; Mg, Cd and Mn)[6]. Then the question arises: can the electrostatic interactions between DNA wrapped in NCPs affect the positional and orientational order of NCPs in dense phases? One can expect that a *matching* of DNA charge patterns takes place along *side-to-side* contacts of neighbouring NCPs; see figure 3. Indeed, x-ray crystal data show that DNA wrapped in NCPs keeps the register of minor grooves on consecutive DNA turns forming a so-called DNA '*supergroove*' [44].

[5] The phases observed at high pressures without divalent Mn cations [10]—which are essential for the crystallization of NCPs, occupying definite sites in NCP crystals and participating in top-to-bottom interactions between NCPs [2, 16] and also possibly affecting DNA–DNA interactions on neighbouring NCPs—do not imply the optimization of NCP–NCP interactions. Thus, the NCP organization in these phases should not necessary be the same as in real NCP crystals. Therefore, it is not surprising that NCP frustrations progressively develop in dense phases under stress as the concentration of PEG increases [10].

[6] These cations bind preferentially into the major groove of DNA neutralizing its charge to a large extent. In the theory, this major-groove cation binding causes a better axial charge separation and strengthens DNA–DNA attraction (binding into a minor groove can also cause an attraction, although a weaker one). DNA helices repel each other in a solution of NaCl, presumably because of comparably weak DNA charge neutralization by Na^+ and its attraction-unprofitable binding on DNA (into the minor groove [43]).

To understand some effects of DNA charge matching on NCP–NCP electrostatic interactions, let us consider DNA as a *circle* wrapped around the histone proteins (the opening/pitch angle of the DNA superhelix in NCP is *on average* ∼5–6° (see footnote 4)); figure 3. At physiological ionic strength (a Debye screening length of $1/\kappa \sim 7$ Å) only the fragments of wrapped DNA near the NCP–NCP contact interact efficiently. Interactions of DNA fragments further apart from the contact region are exponentially screened as well as the interaction between the positively charged histone cores. The interaction of DNA charges near the contact is thus expected to result in an *oscillating* NCP–NCP interaction potential upon the azimuthal rotation of one of the NCPs. We predict that, due to a DNA helical charge motif, the preferred *mutual* azimuthal orientations of neighbouring NCPs positioned across and along the bilayer become *quantized* by an angle $\approx\pi/4$, i.e.

$$\alpha_{i+1} - \alpha_i = k_i\pi/4, \qquad \alpha_{i+2} - \alpha_i = m_i\pi/4, \tag{1}$$

where k_i and m_i are integers; see figure 1. This is the main prediction of the paper. These NCP preferential orientations occur because there are about eight full DNA helical turns per DNA superhelical turn in NCPs; see figure 1(d) in [2] and figure 3. Thus, the zipper-like registration of positive and negative charges on the contacting sides of two NCPs occurs upon the mutual rotation on every $2\pi/8$ around the histone 'cylinder' axis. Since the number of DNA turns is even (eight), no NCP azimuthal frustrations are required to optimize the interaction energy. If this number were odd, then, similarly to hexagonal lattices of parallel DNAs [30], NCP azimuthal frustration on lattices would be required. In the next section, we estimate the magnitude of the effect imposed by this symmetry argument.

One of the effects that can weaken our predictions is the *sequence dependence* of DNA helical base pair parameters [2, 45], of the number of bases per superhelical turn, and of DNA superhelical pitch. Note also that, in reality, a non-complete DNA wrapping around the histone core ($1\frac{3}{4}$ DNA turns) can result in the fact that only a couple of k_i values will be realized—those that preserve strong contacts along and across the bilayer between the NCP sides with two DNA turns; figure 1. At larger NCP dyad axis fluctuations, weaker 2:1 or 1:1 DNA–DNA contacts can emerge. We propose also that side-to-side NCP–NCP electrostatic interactions are dominated by DNA–DNA interactions at $1/\kappa \sim 10$ Å. Thus, the NCPs should interact two to four times stronger through their sides with two DNA turns compared to interaction of the sides with a single DNA turn. This is one of the factors that can drive the bilayer formation and modulate the nucleosomal density in dense phases. The actual value of this force enhancement factor depends on the value of κ, on NCP–NCP separation, and on separation between DNA turns on the NCP; see the next section and figure 7.

3. Debye–Hückel model for NCP–NCP electrostatic interactions

3.1. Charged stripes on planar surfaces

The quantitative theory of electrostatic interaction of DNA superspirals on NCPs is desirable for arbitrary orientations of NCPs, which is, however, a complicated mathematical problem. Below, we try to estimate the energy of electrostatic interaction of NCPs for a particular situation when NCPs are contacted side-to-side by their DNA. To do this, we calculate the interaction energy of planar arrays of parallel alternating inclined stripes of negative (red) and positive (blue) point-like charges, figure 4, which are supposed to mimic DNA phosphates and cations adsorbed on DNA, respectively. A mutual horizontal shift of these charged arrays (unrolled NCPs) mimics the mutual azimuthal rotation of NCPs. The separation between these charged sheets is z, and the charge–charge distance along the stripes is ∼7 Å (the distance

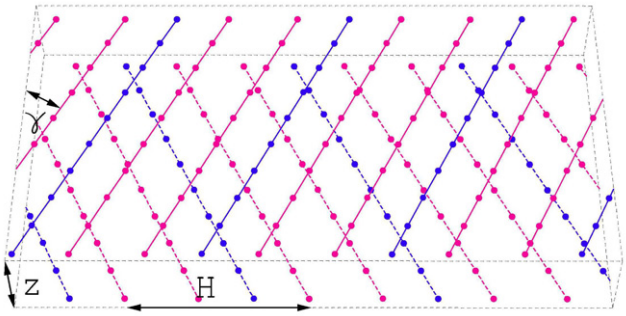

Figure 4. Schematic distribution of charges on two interacting stripes of charges representing unrolled NCPs; DNA phosphates are in red; cations adsorbed in a DNA major groove are in blue.

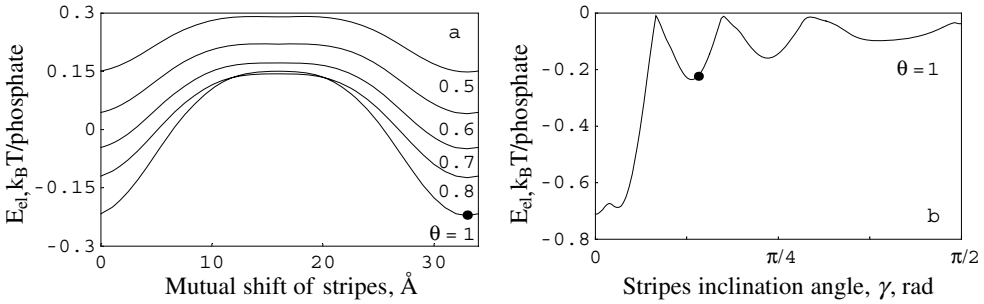

Figure 5. Electrostatic interaction energy between charged stripes as follows from equation (2) (a) as a function of the mutual shift of upper sheet with respect to the lower sheet at $\gamma \approx 25°$ for different values of θ and (b) as a function of stripe inclination angle γ for $\theta = 1$. The points marked in these two graphs correspond to the same conditions. For both figures, $z = 7$ Å and $\kappa^{-1} = 7$ Å.

between phosphates along a strand of B-DNA). The inclination angle γ of charge stripes form with the 'NCP axis' is set to $\gamma \approx 25°$ using the pitch angle of B-DNA ($\sim$30°) and the superhelical angle of DNA in NCP ($\sim$5–6°). We set ten charges per stripe because the DNA has $\approx$10 phosphates per turn and there are two DNA turns for NCP contacts inside the bilayer. The height of the DNA minor groove is $2H/5$, where $H = 34$ Å, and we account for this building the charge arrays. For clarity of presentation in the picture we set that cations adsorb only in DNA major groove, neutralizing fraction θ DNA charge. The realistic θ value for DNA in solution is $\sim$0.8 in a solution of simple salt [46], depending strongly, however, on the salt conditions and counterion valence. In the text, we study the effects of DNA occupation by the adsorbed cations. In our estimation, we neglect the effects of low-dielectric cores of DNA and of NCP when summing the charge–charge interactions in equation (2), assuming a dielectric continuum with $\varepsilon = 80$ everywhere; the effect of DNA helicity is also simplified upon such charge 'unrolling'.

We approximate the interaction energy of charge arrays by the sum of Debye–Hückel electrostatic potentials between all charges:

$$E_{\mathrm{el}} = k_{\mathrm{B}} T l_{\mathrm{B}} \sum_{i,j} \mathrm{e}^{-\kappa r_{ij}} / r_{ij}. \tag{2}$$

Doing the summation, we obtain that, at high fractions of charge neutralization, an attraction of charged stripes is observed for some inter-plane distances z. This attraction is caused by a

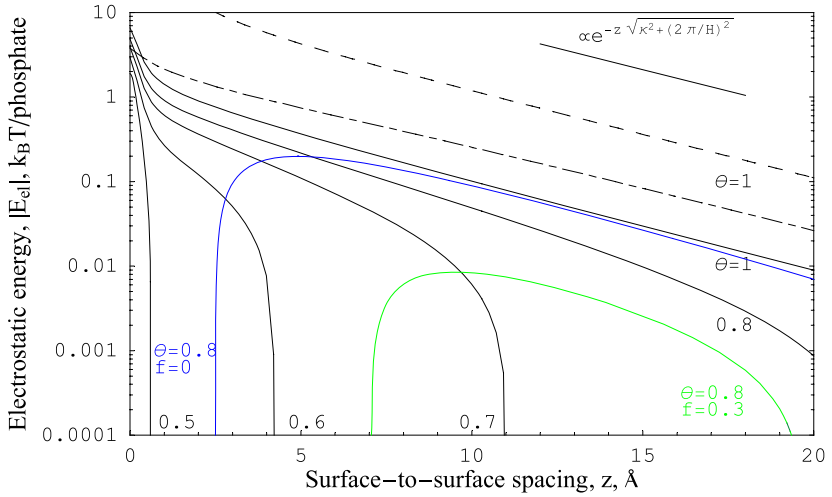

Figure 6. The energy of electrostatic attraction as a function of surface-to-surface separation z at the best mutual allignment of inclined stripes of discrete charges with $\gamma \approx 25^\circ$ as given by summation of Debye–Hückel interaction potentials (equation (2), solid curves) and for planes with continious charged lines with $\gamma = 0$, $\theta = 1$ as calculated analytically (equation (5), dot–dashed curve) and numerically according to equation (2) (dashed curve). Interaction energy of two parallel DNA helices at $\theta = 0.8$ and for different cations' partitioning on DNA: $f = 0$ for blue curve (all cations are adsorbed in DNA major groove); $f = 0.3$ for green curve (30% of cations are in the minor and 70% are in the major groove).

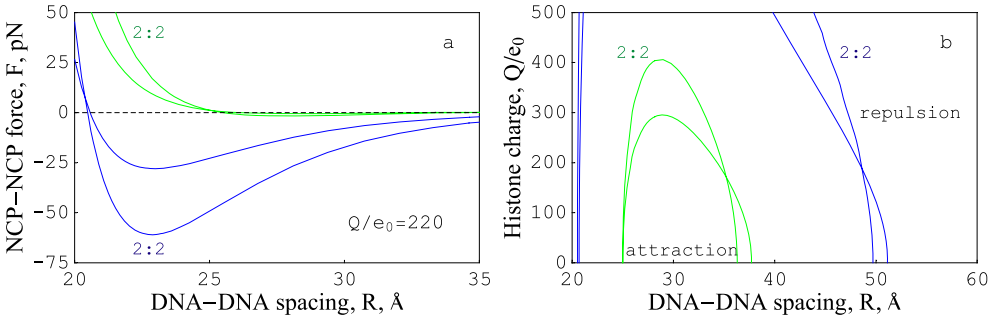

Figure 7. (a) Electrostatic force NCPs as a function of NCP–NCP surface-to-surface distance, $R - 2a$. (b) NCP–NCP electrostatic repulsion–attraction phase diagram as a function of the histone core charge and NCP–NCP separation. The curves calculated for interactions of NCP sides with two DNA turns are marked in the figures as '2:2'; non-marked curves correspond to NCP–NCP interactions by 1:1 DNA sides. Other parameters and notations for the curves are the same as in figure 6; $k_B T/\text{Å} \approx 40$ pN.

proper in-phase matching of positive and negative charge patches on interacting charge arrays; figure 5(a). For non-complete charge neutralization, there is a critical separation z_* above which no attraction is observed; figure 6. This critical separation increases as the neutralization fraction θ approaches unity. For values of γ plausible for NCPs, the interaction energy as a function of the mutual shift of charged sheets has a single minimum that corresponds to *correlation-induced attraction*. The E_{el} at optimal mutual alignment depends on γ, being typically larger for smaller γ when a better registration of charges can be achieved; figure 5(b). In the appendix, we present the analytical results for a particular case of interaction of planar arrays of alternating continuous charged lines at $\gamma = 0$.

In this model, the typical interaction energy for a surface-to-surface distance of 7–10 Å appears to be $\sim$0.01–0.2k_BT per phosphate. The strength of attraction at optimal mutual positioning of stripes decays nearly exponentially with z with the decay length

$$1/\sqrt{\kappa^2 + (2\pi/H)^2} \tag{3}$$

that accounts for electrolyte screening and for the effect of surface charge periodicity. This decay length is shorter than the Debye decay length $1/\kappa$ of electrostatic repulsion of uniformly charged objects in electrolyte solution.

In figure 6 we also show analytical results for the interaction of two planes with straight ($\gamma = 0$) continuous thin charged lines (positive and negative lines are equidistant and $\theta = 1$) derived as a solution of the linear Poisson–Boltzmann equation (dotted–dashed curve in figure 6, equation (4) in the appendix). We have matched the density of negative charges for both cases close to that of *B*-DNA, $\sim -e_0$ nm^{-2}.

We show also for comparison the interaction energy of two parallel DNA duplexes at a typical value of $\theta = 0.8$ and at two different cation partitionings on the DNA surface (the blue curve in figure 6 is for $f = 0$ and the green curve is for $f = 0.3$). The blue curve corresponds to a stronger DNA–DNA attraction according to DNA–DNA electrostatic interaction theory because all cations are adsorbed in the DNA major groove; see [27]. Attraction between DNA exists also for $f = 1$, i.e. when all adsorbed cations occupy the DNA minor groove, but it then requires higher DNA charge neutralization fractions. Note that, at short separations, the DNA–DNA attraction is weakened and it turns into repulsion due to a consistent treatment of DNA low-dielectric cores in the theory of DNA–DNA interaction. In figure 6, we have taken into account the first three helical harmonics of DNA–DNA interaction energy; equation (5) in [30].

3.2. DNA-mediated electrostatic forces between NCPs

We have estimated the electrostatic *force* between the sides of NCPs with two and one DNA turns, figure 7(a), at *optimal* DNA–DNA azimuthal alignment. Histone octamers have been modelled here as homogeneously charged spheres with a radius of $a_h = 35$ Å and charge of $Q = +220e_0$, which repel each other according to the electrostatic theory of double-layer repulsion [47]. For DNA, we set $\theta = 0.8$ independently on the histone charge (see [48] for a model of DNA–histone charge coupling). We have used the Derjaguin approximation [47] in order to restore the force acting between the curved DNA segments in NCPs from the interaction energy of parallel DNA helices [26, 29, 30]. For simplicity we set that DNA turns are in registration on interacting NCPs; the separation between DNA turns on NCP is $l = 28$ Å, as the NCP crystal structure reveals [2]. So, the separations between the axes of interacting DNAs are R and $\sqrt{R^2 + l^2}$. We obtain that the electrostatic force between NCPs is repulsive at short surface-to-surface NCP–NCP separations ($R - 2a$), as dictated by strong image-charge repulsion originating from the interaction of DNA. At intermediate distances, the force can be attractive due to attraction between DNA. At large distances, the NCP–NCP interactions are again repulsive—at such distances DNA–DNA attraction decays, being screened with a shorter screening length than the Debye–Hückel repulsion of homogeneously charged histone cores. As one could expect, electrostatic attraction between NCPs is more pronounced when they interact via the sides with two DNA turns. The actual position of this attractive region crucially depends on the parameters used for DNA–DNA interactions (θ and f) as well as on the histone charge Q/e_0. To study the effect of the histone charge, in figure 7(b) we plot this NCP–NCP attraction–repulsion state diagram as a function of the distance between DNA on interacting NCPs R. As one can see, there is a critical histone charge above which

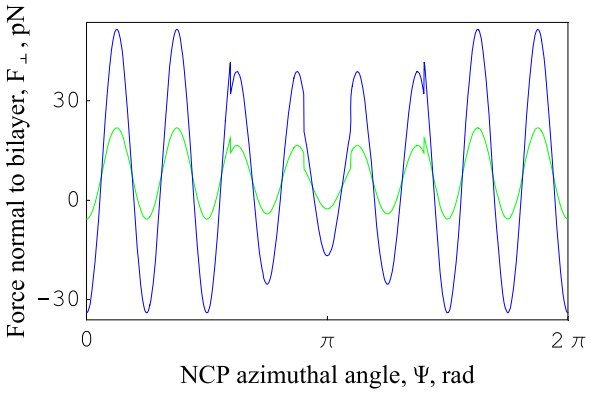

Figure 8. Electrostatic force acting on NCP from the two neighbouring NCPs across the NCP bilayer at $R = 30$ Å (or ∼10 Å between outer NCP surfaces). Other parameters and notations for the curves are the same as in figure 6.

no attraction between NCPs takes place; this critical charge is larger when NCP sides with two DNA turns interact.

We have estimated the force acting on NCP in a direction perpendicular to the bilayer (originating from two neighbouring NCPs) as a function of its azimuthal rotation; figure 8. The dyad axes of neighbouring NCPs were fixed to point into the solution, perpendicular to the bilayer plane. The number of DNA–DNA contacts is calculated for every orientation angle Ψ of the first NCP along the line connecting the centres of NCPs (this can result in artificial jumps in force for such values of Ψ when the number of DNA–DNA contacts changes abruptly, being either 2:2 or 2:1 or 1:1). We considered the case when $1\frac{3}{4}$ DNA turns are wrapped and there are eight DNA turns per superhelical turn. The axis-to-axis DNA–DNA separation near NCP–NCP contact is set to $R = 30$ Å in this figure, both for NCPs along and across the bilayer that correspond to ∼120 Å separation between NCP centres, close to the distances measured experimentally [18]. At this separation, DNA attraction exists both for $f = 0$ and $f = 0.3$; see figure 6. In figure 8, only the *first* azimuthally dependent $\cos(\delta\varphi)$ term in the DNA–DNA interaction energy [30] has been used for clarity (the next term usually has much smaller magnitude and results in a $\cos(2\delta\varphi)$ dependence of the interaction energy). As one could expect, the force oscillates between negative and positive values following the periodic $\pi/4$ variation coming from the DNA–DNA interaction energy, figure 8, which supports the prediction of equation (1). For Ψ close to π, there are two 2:1 DNA–DNA contacts across the bilayer and the force drops two-fold compared with the case of two 2:2 contacts for small values of Ψ. This asymmetry in interaction implies that new NCP phases might exist, as we discuss in section 4. As we have already noted, the strength of NCP–NCP interactions depends on θ, f, and Q/e_0, and one should take the force magnitudes in figure 8 with caution. The periodicity of oscillations of the NCP–NCP force is, however, largely independent of these parameters, being a consequence of DNA spirality and the geometry of its superhelical wrapping in the NCP.

4. Discussion and outlook

4.1. NCP bilayers

The interaction energy (per charge) for two arcs of curved DNA in NCPs is expected to be smaller than our estimates for planar arrays of charged stripes because the charge–charge separations increase due to the curvature. The intensity of NCP–NCP interactions will depend

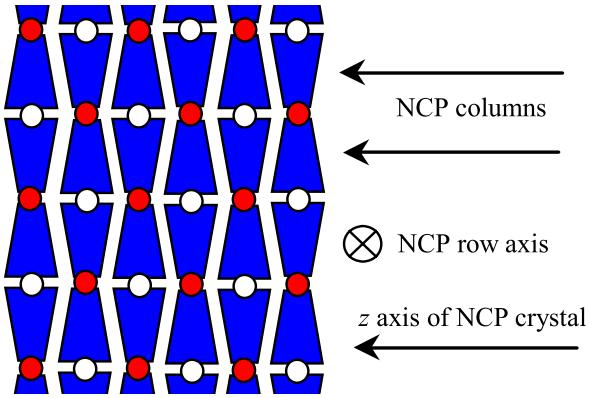

Figure 9. NCP crystal of wedge-shaped core particles. 2:2 and 1:1 DNA–DNA contacts on neighbouring NCP columns are marked white and red circles, respectively. Up and down NCP dyad orientations alternate both along NCP columns and between NCP rows. All NCPs in a row have the same orientations.

on the actual number of charges which are closer to NCP–NCP contact than one Debye screening length, $\kappa^{-1} \sim 7$ Å at physiological conditions. For separations of ∼7 Å between outer NCP side surfaces, this estimate results in ∼10 charges per NCP that results in ~ 0.1–$2k_BT$ electrostatic pinning potential for azimuthal rotations in a pair of NCPs (depending on the parameters chosen). This is, however, a rough estimate. More reliable values should be obtained from the exact theory of electrostatic interaction of realistic NCPs, with superhelical positioning of DNA charges, with a pattern of histone charges, and in the presence of low dielectric cores of DNA and histones. This remains, however, a complicated mathematical problem which can be the subject of future research.

As figure 1(b) shows, there is already some experimental evidence of NCP azimuthal frustration in bilayers. The quantitative analysis of these fluctuations can provide additional information on the magnitude and azimuthal dependence of NCP–NCP interaction potential. Mutual NCP azimuthal correlations across the bilayer can, in principle, be extracted from cryo-electron micrographs of Leforestier *et al* [18], provided that better statistics and resolution are achieved. Note, however, that in this recent paper the experimental group stated that their data 'yield no information about possible correlations between NCPs belonging to the two layers of a given bilayer' [10]. If this correlation function has peaks separated by $\sim\pi/4$, our predictions are valid. Then, more elaborate NCP–NCP interaction potentials have to be implemented to treat the effect quantitatively. To separate the effects of NCP tails versus the effects of DNA charge non-homogeneity on NCP–NCP interactions, one can suggest studying the bilayer formation with modified (acetylated) NCP tails. The phase boundaries are also shifted after a partial deletion of the histone tails and after a change of the length of wrapped DNA [10]. It was suggested that the phase equilibrium is controlled by the total *charge* of the DNA–histone complex [10], but no unambiguous conclusions have been made.

4.2. Other NCP phases

Our results for NCP bilayers could also give some insight into the electrostatic contribution in driving forces for NCP crystallization. In NCP crystals, no NCP azimuthal frustration is observed (presumably, too strong inter-nucleosomal interactions do not allow them to occur) and NCP lateral organization is reminiscent of that in bilayers, provided that the layer of solvent

is removed artificially. Namely, the 2:2 DNA–DNA contacts alternate with 1:1 contacts in neighbouring rows of NCPs in the hexagonal crystal layer [16]; figure 9 (differences in crystal organization of NCPs of yeast and frog are discussed in [16]).

Also, a peculiar phase transition from a lamellar phase of NCP bilayers to a quasi-hexagonal crystalline phase experimentally observed at ∼50 mM of NaCl [9] might be of electrostatic nature. One can suggest that, similar to the lamellar phase of charged amphiphilic molecules, at low salt, the NCP bilayer phase is electrostatically stabilized, while at higher ionic strength the repulsion of layers is diminished, allowing denser crystalline phases to emerge. Similarly, colloidal crystals form typically denser phases when interparticle interactions become shorter range [49][7]. Another possible effect of salt can be that, with an increase in salt concentration, cations neutralize NCPs better and thereby diminish their mutual repulsion[8]. Note here that pressure-induced lamella to inverse-hexagonal phase transition observed for NCP assembly is reminiscent of that for amphiphilic molecules [50, 51]. One could further extend the analogy with amphiphiles, where the preferred phases are determined by the geometric shape of elementary units (cylinder, cones, inverted cones, etc) and their stoichiometric ratio with water. Although for amphiphiles the allowed phases can be rationalized by this method, the understanding of physical origins for transitions between the phases requires additional input and often can be described only phenomenologically [52, 53]. In the case of the NCP inverse hexagonal phase, this transition might be stabilized by the creation of additional 2:2 DNA–DNA contacts at the points where three NCP bilayers are matched together.

Using the analogy with amphiphiles, one can speculate that, depending on the DNA length wrapped in NCPs, new meso-phases of NCP columns might exist which have not yet been detected (in addition to the known phases of individual NCP columns, NCP bilayers, inverse-haxagonal and crystalline phases). Namely, the bilayer phase occurs when at least $1\frac{1}{2}$ turns of DNA are wrapped, while the inverse hexagonal phase and crystalline phase can be stable for $1\frac{1}{2}$–2 wrapped DNA turns. When the DNA wrapping length is $<1\frac{1}{2}$ turns, we expect the *bundles* of NCP columns to be stable, at least at high salt ionic strength when the NCP–NCP interactions are dominated by those of outer DNAs. In this new phase, NCP sides with two DNA turns establish attractive contacts inside the bundle pointing dyad-axis side into the solution. For $\sim 1\frac{1}{3}$ DNA turns one can expect to see hexagonal bundles of about 30 nm in diameter with seven NCP columns aligned in it, while for $\sim 1\frac{1}{6}$ turns the trimers of columns can be stable. Similar preferences to form bundles can be triggered by enhancing the NCP–NCP interactions on the side opposite to the NCP dyad-axis side.

Acknowledgments

We thank A Leforestier for helpful comments and for providing a high-resolution image of NCP bilayers. RE acknowledges support from the ‘chaire d’excellence’ program of the French ‘Agence Nationale de la Recherche’.

[7] Indeed, in the case that NCP bilayers possess a residual electric charge, the electrostatic repulsive pressure between them should decrease with increasing κ [47]. The Debye length in solution of the NCP lamellar phase varies between ∼20 and ∼50 Å, while the bilayer–bilayer distance is much larger, varying from 90 to 220 Å, depending on the initial NCP concentration and PEG pressure. However, simple estimates (a nonlinearized version of equation (5)) show that, even for 90 Å of solvent between the bilayers and for layer charge density close to that of bare *B*-DNA, the disjoint pressure between the layers cannot exceed ∼1 atm, while the phases are observed at ∼5 atm of external stress.

[8] However, if NCPs *can* attract each other via DNA, what prevents bilayers from collapsing onto each other? As figure 7 shows, this can be the repulsion of positive histone cores that results in the repulsive interaction of 1:1 NCP sides, while 2:2 NCP sides still attract each other at short distances. Another possibility is the solvation energy of charged NCPs which are affine to highly polarizable aqueous solution between bilayers.

Appendix. Interaction of periodic planar charge arrays

We calculate below the electrostatic interaction energy of two parallel planes with alternating positively and negatively charged thin charged lines with the period H. In addition, the planes are positively homogeneously charged and separated by distance D. The positive lines compensate a fraction θ of the charge of negative lines and are shifted along axis y by distance s with respect to the negative lines. Coordinate x is along the charged lines (it is irrelevant for further discussion), z is perpendicular to the planes, and y is along the plates and perpendicular to the charged lines. The charge distribution on plane 1 at $z = D$ is shifted along axis y by distance h with respect to the charge distribution on plane 2 at $z = 0$.

The charge density on two planes is $\rho(z, y) = \delta(z)\sigma(y) + \delta(z - D)\sigma(y - h)$, where $\sigma(y) = \sigma_0 + \sigma_1 H \sum_{m=-\infty}^{\infty} \delta(m - y/H) - \theta\sigma_1 H \sum_{m=-\infty}^{\infty} \delta(m - (y - s)/H)$ and $\delta(z)$ is the Dirac delta function. We use the Fourier transformation over y for the electrostatic potential $\phi(z, y)$ and $\sigma(z, y)$, i.e. $\{\phi(z, y), \sigma(z, y)\} = \sum_{n=-\infty}^{\infty} \mathrm{e}^{-ingy}\{\tilde{\phi}_n(z), \tilde{\sigma}_n(z)\}$, where $g = 2\pi/H$. The Poisson–Boltzmann equation in 1:1 electrolyte solution with concentration of salt n_0 is $(\mathrm{d}^2/\mathrm{d}y^2 + \mathrm{d}^2/\mathrm{d}z^2)\phi(z, y) = \kappa^2\phi(z, y)$, and has the solution $\tilde{\phi}_n(z) = A_n\mathrm{e}^{-\kappa_n z} + B_n\mathrm{e}^{\kappa_n z}$, where $\kappa = \sqrt{8\pi l_B n_0}$, $\kappa_n = \sqrt{\kappa^2 + n^2 g^2}$ and A_n and B_n are found from the boundary conditions.

The interaction energy of two surfaces is $E_{\mathrm{int}}(D) = E_{\mathrm{el}}(D) - E_{\mathrm{el}}(\infty)$, where $E_{\mathrm{el}}(D) = \frac{1}{2}\int \mathrm{d}z \sum_{n=-\infty}^{\infty} \tilde{\phi}_n(z)\tilde{\sigma}_{-n}(z)$. Thus, we get that, per unit surface area, $E_{\mathrm{int}}(D)$ is the sum of the interaction energy of homogeneously charged planes with the net charge density and corrections due to the discreteness of charge patterns:

$$E_{\mathrm{int}}(D) = \frac{4\pi[\sigma_0 + \sigma_1(1-\theta)]^2}{\varepsilon\kappa}\frac{1 + \mathrm{e}^{-\kappa D}}{\sinh[\kappa D]} + \frac{8\pi\sigma_1^2}{\varepsilon}\sum_{n=1}^{\infty}\frac{(1 + \theta^2 - 2\theta\cos[ngs])}{\kappa_n}\frac{\cos[ngh] + \mathrm{e}^{-\kappa_n D}}{\sinh[\kappa_n D]}. \tag{4}$$

For $n = 1, \theta = 1$, and at $s = h = H/2$, this correction term results in attraction between the surfaces: positive strings on one surface are opposite to negative strings on another surface. This correlation-induced attraction decays nearly exponentially with D, with a decay length of κ_1^{-1}. In the limit of $\kappa D \gg 1$ and for low surface charge densities, the first term in equation (4) turns into the known expression [47]

$$E_{\mathrm{int}}(D) \approx 4n_0 k_B T \kappa^{-1} \Psi_0^2 \mathrm{e}^{-\kappa D}, \tag{5}$$

where the surface potential (assumed to be small) is $\Psi_0 = 4\pi\sigma_0 e_0/(\varepsilon\kappa k_B T)$. Note that this linear theory, as well as the Debye–Hückel model of equation (2), break down near highly charged surfaces.

References

[1] Richmond T J *et al* 1984 *Nature* **311** 532
[2] Luger K, Maeder A W, Richmond R K, Sargent D F and Richmond T J 1997 *Nature* **389** 251
[3] Dorigo B *et al* 2004 *Science* **306** 1571
[4] Schalch T, Duda S, Sargent D F and Richmond T J 2005 *Nature* **436** 138
[5] Robinson P J J, Fairall L, Van Huynh A T and Rhodes D 2006 *Proc. Natl Acad. Sci. USA* **103** 6506
[6] Widom J 1998 *Annu. Rev. Biophys. Biomol. Struct.* **27** 285 and references therein
[7] Calladine C R, Drew H R, Luisi B F and Travers A A 2004 *Understanding DNA* (Amsterdam: Elsevier)
[8] Rossetto V and Everaers R 2006 in preparation
[9] Mangenot S, Leforestier A, Durand D and Livolant F 2003 *Biophys. J.* **84** 2570
[10] Mangenot S, Leforestier A, Durand D and Livolant F 2003 *J. Mol. Biol.* **333** 907

[11] Leforestier A, Fudaley S and Livolant F 1999 *J. Mol. Biol.* **290** 481
[12] Livolat F *et al* 2006 *Phil. Trans. R. Soc.* A **364** 2615 and references therein
[13] Finch J T and Klug A 1977 *Cold Spring Harbor Symp. Quant. Biol.* **42** 1
[14] Finch J T *et al* 1977 *Nature* **269** 29
[15] Finch J T *et al* 1981 *J. Mol. Biol.* **145** 757
[16] White C L, Suto R K and Luger K 2001 *EMBO J.* **20** 5207
[17] Dubochet J and Noll M 1978 *Science* **202** 280
[18] Leforestier A, Dubochet J and Livolant F 2001 *Biophys. J.* **81** 2414
[19] Leforestier A, private communication
[20] Luger K and Richmond T J 1998 *Curr. Opin. Genet. Dev.* **8** 140
[21] Mangenot S, Raspaud E, Tribet C, Belloni L and Livolant F 2002 *Eur. Phys. J.* E **7** 221
[22] Lorman V, Podgornik R and Zeks B 2005 *Europhys. Lett.* **69** 1017
[23] Mühlbacher F, Holm C and Schiessel H 2006 *Europhys. Lett.* **73** 135
[24] Cherstvy A G and Winkler R G 2006 *J. Chem. Phys.* **125** 064904
Cherstvy A G and Winkler R G 2006 *Phys. Rev. Lett.* **96** 066103
See also Cherstvy A G and Winkler R G 2004 *J. Chem. Phys.* **120** 9394
[25] Mangenot S, Leforestier A, Vachette P, Durand D and Livolant F 2002 *Biophys. J.* **82** 345
[26] Kornyshev A A and Leikin S 1997 *J. Chem. Phys.* **107** 3656
[27] Kornyshev A A and Leikin S 1999 *Phys. Rev. Lett.* **82** 4138
[28] Kornyshev A A and Leikin S 2001 *Phys. Rev. Lett.* **86** 3666
[29] Cherstvy A G, Kornyshev A A and Leikin S 2002 *J. Phys. Chem.* B **106** 13362
[30] Cherstvy A G, Kornyshev A A and Leikin S 2004 *J. Phys. Chem.* B **108** 6508
[31] Cherstvy A G and Kornyshev A A 2005 *J. Phys. Chem.* B **109** 13024
[32] Kornyshev A A and Leikin S 1998 *Proc. Natl Acad. Sci. USA* **95** 13579
[33] Cherstvy A G 2005 *J. Chem. Phys.* **123** 116101
[34] Poghossian A *et al* 2005 *Sensors Actuators* B **111–112** 470
[35] Cherstvy A G 2005 *J. Phys.: Condens. Matter* **17** 1363
[36] Kornyshev A A, Lee D J, Leikin S, Wynveen A and Zimmerman S B 2005 *Phys. Rev. Lett.* **95** 148102
[37] Rau D C and Parsegian V A 1992 *Biophys. J.* **61** 260
Rau D C and Parsegian V A 1992 *Biophys. J.* **61** 246
Leikin S, Rau D C and Parsegian V A 1991 *Phys. Rev.* A **44** 5272
Leikin S, Parsegian V A, Rau D C and Rand R P 1993 *Annu. Rev. Phys. Chem.* **44** 369
[38] Brenner S L and Parsegian A V 1974 *Biophys. J.* **14** 327
[39] Oosawa F 1971 *Polyelectrolytes* New York
[40] Gronbech-Jensen N *et al* 1997 *Phys. Rev. Lett.* **78** 2477
Nguyen T T, Rouzina I and Shklovskii B I 2000 *J. Chem. Phys.* **112** 2562 and references therein
[41] Strey H H, Wang J, Podgornik R, Rupprecht A, Yu L, Parsegian V A and Sirota E B 2000 *Phys. Rev. Lett.* **84** 3105
[42] Pelta J, Livolant F and Sikorav J-L 1996 *J. Biol. Chem.* **271** 5656
[43] Shui X *et al* 1998 *Biochemistry* **37** 1841 and references therein
[44] Edaysthumangalam R S, Weyermann P, Gottesfeld J M, Dervan P B and Luger K 2004 *Proc. Natl Acad. Sci. USA* **101** 6864
[45] Olson W K, Gorin A A, Lu X-J, Hock L M and Zhurkin V B 1998 *Proc. Natl Acad. Sci. USA* **95** 11163
[46] Manning G S 1978 *Q. Rev. Biophys.* **11** 179
[47] Israelachvili J N 1991 *Intermolecular and Surface Forces* (New York: Academic)
[48] Cherstvy A G and Winkler R G 2005 *J. Phys. Chem.* B **109** 2962
[49] Yethiraj A and van Blaaderen A 2003 *Nature* **421** 513
See also Russel W B 2003 *Nature* **421** 490
[50] Cowley A C *et al* 1978 *Biochemistry* **17** 3163
[51] Rand R P *et al* 1990 *Biochemistry* **29** 76
[52] Gruner S M 1989 *J. Phys. Chem.* **93** 7563
[53] Shearman G C *et al* 2006 *J. Phys.: Condens. Matter* **18** S1105